

Venusian k_2 Tidal Love Number from Magellan and PVO Tracking Data

A. S. Konopliv and C. F. Yoder

Jet Propulsion Laboratory
4800 Oak Grove Drive, Pasadena CA 91109

Abstract. The k_2 potential Love number which scales the tidal deformation of Venus by the Sun has been estimated from Doppler tracking of Magellan and Pioneer Venus Orbiter (PVO) spacecraft data. The nominal range for k_2 from theoretical models is $0.23 < k_2 \leq 0.29$ for a liquid iron core and about 0.17 if the iron core has solidified. Our best estimate of this parameter is $k_2 = 0.2954 \pm 0.066(2\sigma)$ and supports the hypothesis that Venus core is liquid.

Introduction

Inferring internal structure of Venus using orbiting spacecraft data until now has been limited to mass, radius and mean density, with increased accuracy but little additional information than had already been obtained from ground-based radar echo data. The most relevant feature is that Venus appears slightly under dense relative to Earth, and this can either be accounted for in terms of a 4% smaller iron core or a 2% lower density mantle (Ringwood and Anderson 1977). Analysis of Venera lander X-ray fluorescence data suggests an earth-like basaltic crust (Moroz 1983). The absence of an internally generated magnetic field suggests that either the core is entirely liquid (Stevenson *et al.* 1983) or completely solidified (Arkani-Hamed and Toksoz 1984). Venus' slow rotation and mean solar tides raise a hydrostatic oblateness or J_2 gravity coefficient which is about 25 times smaller than the observed $J_2 = 4.42 \times 10^{-6}$ which is primarily due to a combination of topography and internal lateral density variations, the latter which drives mantle convection (c. g. Kiefer *et al.* 1986). Hence the observed J_2 cannot be employed to infer a radial density structure constraint (i.e. polar moment of inertia) as is done for Earth, Mars and the giant planets and some planetary satellites.

The expected Magellan (MGN) Doppler signature from solid tides on Venus is about 0.1 mm s^{-1} and is the same size as the precision as the line-of-sight Doppler measurements averaged over 10 seconds. For long wavelength (on the order of a day) the mean of the Doppler measurements shows scatter at the 0.02 mm s^{-1} level. This measurement offers the opportunity to probe such features as core liquidity, core size, mantle density and mantle rigidity with

considerable sensitivity partly because the model range for k_2 is fairly broad compared to that for the polar moment.

The Love number and core radius for an earth-like core and mantle composition and thermal profile is 0.255 and 3120 km, respectively (Yoder 1995). The effect of varying core radius and mantle rigidity μ on k_2 are nearly independent. The predicted partials k_2 for these two parameters are

$$\begin{aligned} \frac{\mu}{k_2} \frac{\partial}{\partial \mu} k_2 &= -0.63 \\ \frac{R_c}{k_2} \frac{\partial}{\partial R_c} k_2 &= 2.1 \end{aligned} \quad (1)$$

Mantle and core density profiles are fixed for the rigidity partial. For the core radius partial, mantle density profile is also fixed except near the core-mantle boundary. In addition, core mass and density are adjusted to maintain the total mass constraint. A more physical mantle parameter is the molar fraction of magnesium to iron plus magnesium, χ_m (Mg/(Mg + Fe)). Iron is both less rigid and heavier than Mg and both effects conspire to increase k_2 with decreasing χ_m . The partial (holding core radius, but not composition fixed) is

$$\frac{\chi_m}{k_2} \frac{\partial}{\partial \chi_m} k_2 = 0.76 \quad (2)$$

If one limits the maximum variation in $\chi_m = \pm 5\%$ and core density change at core pressures and temperatures to $\pm 0.5 \text{ g cm}^{-3}$ then the maximum range for the Love number is $0.23 \leq k_2 \leq 0.29$, (the predicted moment of inertia range is quite narrow: $0.334 < C/MR^2 < 0.341$) (Yoder 1995). Anelastic softening at the 58.4 d tidal flexing period might increase k_2 by a few per cent. On the other hand if the core has solidified and has a core rigidity of about 1 Mbar, then k_2 is reduced to > 0.17 .

Tidal potential model

The tidal potential acting on a spacecraft at position \mathbf{r}_{st} relative to Venus is $k_2 \frac{GM_{\odot}R^5}{(r_{\odot}r_s)^3} (\frac{3}{2}(\hat{\mathbf{r}}_{st} \cdot \hat{\mathbf{r}}_{\odot})^2 - \frac{1}{2})$ where M_{\odot} is the mass of the Sun, \mathbf{r}_{\odot} is the vector from Venus to the Sun, and R is the equatorial radius of Venus. The equivalent tidal contributions to the normalized second degree gravity coefficients are (e.g. Eanes *et al.* 1983)

$$\begin{aligned} \delta \bar{C}_{2m} &\sim i \delta \bar{S}_{2m} = k_2 A_{nm}(\phi_{\odot}) \exp im\alpha_{\odot} \\ A_{nm}(\phi_{\odot}) &= N_{2m} \frac{GM_{\odot}R^5}{(r_{\odot}r_s)^3} P_{2m}(\sin \phi_{\odot}) \\ N_{2m} &= \sqrt{\frac{(2-m)!(2-\delta nm)}{5(2+m)!}} \end{aligned} \quad (3)$$

where respectively ϕ_{\odot} and α_{\odot} are latitude and longitude of the Sun relative to Venus' figure. The Legendre functions $P_{2m}(\sin \phi_{\odot}) = (\frac{3}{2}\sin^2 \phi_{\odot} - \frac{1}{2}), 3\sin \phi_{\odot} \cos \phi_{\odot}, 3\cos^2 \phi_{\odot}$ for essential order $m = 0, 1, 2$, respectively. Since the Venusian

latitude of the Sun is $<3^\circ$, the only significant time varying terms occur for the $\delta\bar{C}_{22}$ and $\delta\bar{S}_{22}$ coefficients. The expected amplitude for the normalized coefficients for a nominal Love number of 0.25 is 70×10^{-10} for a near Venus orbiter compared to a standard deviation (formal σ) for \bar{C}_{22} and \bar{S}_{22} of 9×10^{-10} for the combined data sets.

Consider the Doppler velocity signal v_s from an orbiting satellite near the planet and in a circular orbit. The radial part which depends on solar longitude $\lambda_{(c)}$ and can be separated from Venusian gravity perturbations is (Yoder 1995)

$$\delta v_{st(\text{radial})} = -k_2 H_{(c)} v_{st} \left(\frac{R}{a_s} \right)^2 C_r(\lambda_{(c)}) - 0.5 k_2 C(\lambda_{(c)}) \text{m/s}, \quad (4)$$

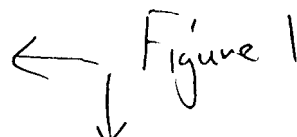
with

$$C(\lambda_{(c)}) = \frac{4 \cos^4 \frac{\pi}{2} I \cos(2\lambda_{st} - 2\lambda_{(c)}) + 4 \sin^4 \frac{\pi}{2} J \cos(2\lambda_{st} + 2\lambda_{(c)} - 4\Omega_{st})}{\sin^2 J \cos(2\lambda_{st} - 2\Omega_{st})} \quad (5)$$

and where $H_{(c)} = (M_{(c)}/M)(R/a)^3$, M , R and a are planetary mass, radius and orbital semi-major axis, respectively. I is the satellite inclination to the equator and λ_{st} and Ω_{st} are satellite mean longitude and node, respectively. Since Venus rotates retrograde, the Venusian solar 'day' is 116.75 earth days, while the primary tidal flexing period is 58.4d.

The two data sets analyzed are outlined by Konopliv and Sjogren (1994) and include the Pioneer Venus Orbiter (PVO) Doppler tracking (orbital $c = 0.8$ with periaxle ranging from a 'high' 1000km to a 'low' 150km) from beginning of mission in December of 1978 to September, 1982 and Magellan Doppler tracking from beginning of the gravity cycles 4 ($c = .04$, periaxle altitude: 170km) and 5 ($c = .02$, apoaixle altitude: 500km) in September 1992 to end of mission in October 1994 during cycle 6. The Venus tidal effect must be separated from other forces that are dependent on the local solar time such as radiation pressure due to Venus albedo and atmospheric drag. In solutions for these forces, the tide generally correlates with orbit parameters describing spacecraft state vector and solar pressure and albedo correlation with drag. The albedo is fairly well determined for the PVO high altitude orbits but the tidal effect is better determined for the low altitude orbits. Figures 1 a and 11, show typical radial acceleration profiles for the Magellan pre- and post-aerobraking orbits, respectively. The drag force is substantially smaller for Magellan than 'low' PVO due to the lower spacecraft velocity through the atmosphere. The tidal force is about 4 times greater than the albedo force. Separation of the tidal signature can be achieved partly because the tidal force remains the same on the nightside of Venus while the albedo force vanishes and the drag force diminishes by an order of magnitude. The Magellan Doppler data at X-band (8.435 GHz) is an order of magnitude less noisy than PVO S-band (2.2 GHz) data.

The solution procedure (Konopliv *et al.* 1993) first involves breaking the Doppler tracking data (several million observations) into dynamically continuous time spans or data arcs for processing (over 800 arcs). Arcs are up to 10

 Figure 1

days in length for PVO data and are generally one day for Magellan. Both 'local' and 'global' parameters are estimated for each arc. Arc dependent dynamic local forces estimated for Magellan in the general order of their importance are spacecraft state, atmospheric densities (for spacecraft drag), velocity deltas from momentum wheel despinnings, solar radiation pressure coefficients, small velocity increments for star calibrations, acceleration vectors for spacecraft orientation changes to heat or cool down the spacecraft, Venus albedo and Doppler biases.

Nominally, the following global parameters are estimated: the gravity field to degree and order 40, the gravitational constant times the mass of Venus (GM), the ephemerides of the Earth and Venus (12 parameters), and the tidal k_2 Love number. The global gravity model of Venus is determined to about degree and order 40 (Konopliv and Sjogren, 1994) and is the rationale for choosing this degree cutoff. However, to investigate the sensitivity of the Love number solution, the full gravity field is estimated for various degree and orders (with a maximum of 90 or 8278 parameters). The terms of the gravity field beyond the degree and order being estimated are fixed to the nominal gravity solution (a 90th degree field). All gravity solutions are constrained by an a priori of $1.2 \times 10^{-5}/n^2$ (Kaula, 1966) except for one 90th-degree solution with a spatially varying a priori condition as outlined by Konopliv and Sjogren (1995). Also Venus' pole and rotation rate are either estimated or are fixed by the radar imaging (SAR) (e.g., Davies et al., 1992). Fixed pole solutions will eventually be preferred once SAR-determined pole orientation employs improved spacecraft ephemeris modeling.

The observations are processed using a square root information weighted least squares filter (Bierman, 1977) with numerically stable orthogonal Householder transformations (or modified Givens transformations) used to triangularize (i.e. pack) the observations. The global parameters are determined with a technique (Kaula, 1966; Ellis 1980) that merges only the global parameter portion of the square root information arrays from all the data arcs, but is equivalent to solving for the global parameters plus local parameters of all arcs.

Love Number Solution

Table 1a lists the Love number solutions for different data combinations and the estimation of a 40th degree and order gravity field. The nominal k_2 Love number solution with the combined data sets (PVO and MGN cycles 4 and 5 plus 6) and a realistic error (twice the formal standard deviation) is

$$k_2 = 0.2954 \pm 0.066 \quad (\text{eq. 1})$$

The estimated pole solution is chosen since the statistics indicate there is improved pole determination over the radar imaging (SAR) values. Table 1b lists the Love number solutions for estimation of different degree and order gravity

fields as a test of solution stability. The MGN cycle 4 data is from a highly elliptical orbit and the gravity field is less well determined near Venus' poles. The Love number solutions when estimating a low degree field (20, 30, 40) are stable. However, the discrepancy between the fixed and estimated pole solutions progressively increases as degree increases from 50 to 90 due to overestimation of the gravity field.

Since the gravity field from MGN cycles 5 and 6 (a near circular orbit) is better determined on a global scale, this solution is more stable as degree increases. When all data is included in the solution, the solutions are also stable as a function of degree. We, however, as a precaution, provide a realistic uncertainty for k_2 of twice the formal σ since solutions for the individual gravity coefficients can vary by more than $2-3 \times \sigma$ for different data combinations.

From eqs. 1 and 2, a nominal $k_2 = 0.29$ implies that either the mantle is more iron rich than earth's mantle with $\chi_m = 0.74$ (compared to an earth-like value of 0.89) or the core is larger than 31.20 km radius by about 200 km and is less iron rich than earth's core (that is, the Venusian core has a higher percentage of light alloy as compared to earth's core).

The above results support the hypothesis that Venus' core is liquid counter to some Venusian thermal cooling models which predict a solid core (Arkani-Hamed and Toksöz 1984). The fluidity of the core discriminates between models developed to explain Venus' free obliquity (Yoder 1995).

Future prospects

The Doppler residuals from Magellan cycles 5 and 6 data sets will show substantial gravity signatures due to its near circular orbit which definitely affects the orbital parameters for Venus and may affect k_2 . The Doppler bias solutions correlate with the strong gravity signatures of the Aita and Beta regions. Current plans are to solve for a 120 degree and order field with longer 3 day data arcs and better modeling constraints and media calibrations. The first element should improve modeling of cycles 5 and 6 gravity data and the second should improve spacecraft orbit stability.

No new mission to Venus which involves orbiting spacecraft and/or surface lander is presently contemplated. Therefore the only reasonable expectation for improvement in the Love number determination must come from improved modeling of the Magellan data. Although the above changes in analysis may reduce the scatter seen in Table 1, it is unlikely to reduce the formal sigma, in fact it may slightly increase it. A more remote modelling change which requires considerable effort to implement is to consider a new data type, *integrated* Doppler (i.e. different al range). This technique might increase the low frequency resolving power of the data. However, the solar plasma (red) noise character will limit its usefulness (Woo 1975).

Table 2 lists the expected tidal Doppler signature seen by a spacecraft orbiting near the surface of the terrestrial

Table 1

Table 2

planets, Moon and other satellites. This list indicates that this measurement can be pursued in future space missions as advocated by Wu *et al.* (1995) for Mercury and by Hilton (1992) for Mars. Improvements in the radio tracking systems (both Doppler and range) and potential instrument additions such as spacecraft accelerometers to directly measure the nongravitational forces should be pursued and this k_2 parameter along with the permanent gravity field should be a priority for consideration in mission design.

Acknowledgments:

We thank the reviewers (including Bill Kaula) for helpful comments. The Cray Supercomputer funding came from the NASA Offices of Mission to Planet Earth, Aeronautics, and Space Science. The filtering software on the Cray was written by Chuck Lawson and thanks to Fred Krogh for help with the numerical integration. The research described in this paper was carried out by the Jet Propulsion Laboratory, California Institute of Technology, under a contract with the National Aeronautics and Space Administration.

References

- Arkani-Hamed, J. and M. N. Toksoz 1984. Thermal evolution of Venus, *Phys. Earth Planet. Inter.*, 34, 232-250, 1984.
- Bierman, G. J., *Factorization Methods for Discrete Sequential Estimation*, Academic Press, New York, 1977.
- Davies, M. E., T. R. Colvin, P. G. Rogers, P. W. Chodas, W. L. Sjogren, E. L. Akim, V. A. Stepanyantz, Z. P. Vlasova and A. I. Zakharov, The rotation period, direction of the north pole, and geodetic control network, *J. Geophys. Res.*, 97, 13141-13152, 1992.
- Eanes, R. J., B. Schutz and B. Tapley, Earth and ocean tide effects on Lageos and Starlette, in *Proceedings of the Ninth International Symposium on Earth Tides*, F. Schweizer - bair'sche Verlagsbuchhandlung, Stuttgart, 1983.
- Ellis, J., Large scale state estimation algorithms for DSN tracking station location determination, *J. Astronaut. Sci.*, 28, 15-30, 1980.
- Hilton, J. L., The motion of Mars' pole. II: The effect of an elastic mantle and a liquid core, *Astron. J.*, 103, 619-637, 1992.
- Kaula, W. M., *Theory of Satellite Geodesy*, Blaisdell, Waltham, MA., 1966.
- Kiefer, W. S., M. A. Richards, and B. Hager, A dynamic model of Venus' gravity field, *Geophys. Res. Lett.*, 13, 14-17, 1986.
- Konopliv, A. S., N. J. Borderies, P. W. Chodas, E. J. Christensen, W. L. Sjogren, B. G. Williams, G. Balmino, and B. G. Barriot, Venus gravity and topography: 60th degree and order model, *Geophys. Res. Lett.*, 20, 2403-2406, 1993.
- Konopliv, A. S. and W. L. Sjogren, Venus Spherical harmonic gravity field to degree and order 60, *Icarus*, 112, 42-54, 1994.

- Konopliv, A. S. and W. L. Sjogren, The JPL Mars Gravity Field, Mars50c, Based Upon Viking and Mariner 9 Doppler Tracking Data, JPL Publication 95-5, Jet Propulsion Laboratory, Pasadena, CA, February, 1995.
- Moroz, V. I., Results of Veneras 13 and 14 in Venus (Hunten, D. M., Colin, I., Donohue, T. M. and Moroz, V. I. eds.), U. of Ariz. Press, 45-68, 1983.
- Ringwood, A. E. and D. L. Anderson, Earth and Venus: a comparative study, *Icarus*, 30, 243-253, 1977.
- Woo, R., Multifrequency techniques for studying interplanetary scintillations, *Astrophys. J.*, 201, 238-248, 1975.
- WO, X., I'. L. Bender and G. W. Rosborough, Probing the interior of Mercury from an orbiter plus single lander, *JGR Planets*, 100, 1515-1525, 1995.
- Yoder, C. F., Venus' Free Obliquity, *Icarus*, 117, 250-286, 1995.

Alex Konopliv ms 301-125J, Jet Propulsion Lab, 4800 Oak Grove Drive, Pasadena CA 91109, pb 818-354-6105, email: ask@kratijpl.nasa.gov. Charles F. Yoder (JPL), 1115 183-501, pb: 818-354-2444; fax 818-354-0966, email: Charles.F.Yoder@ccmail.jpl.nasa.gov.

(received October 23, 1995;
revised February 29, 1996;
accepted April 10, 1996.)

KONOPLIV AND YODER: VENUSIAN TIDAL LOVE NUMBER

Figure 1. Predicted spacecraft acceleration due to tides (nominal $k_2 = 0.25$), drag and albedo for MGN cycle 4 (1 a) and cycles 5 and 6 (1 b) evaluated at noon, local Venusian time.

Table 1a: Potential k_2 Love number solutions with a 40th degree and order gravity field

	Fixed Pole <i>Davies et al.</i> (1992)	Estimated Pole & Rotation Rate
Data		
PVO	0.2114 0.244	0.2303 0.244
Cycle! 4	0.2493 0.134	0.2454 0.134
PVO+Cyc. 4	0.3224 0.093	0.279 ± 0.093
Cycles 5&6	0.289 ± 0.061	0.3014 0.062
MGN	0.311 ± 0.034	0.3143 0.034
PVO+MGN	0.2894 0.033	0.2953 0.033

Table 1b: Variability in k_2 due to gravity field degree and Venus pole and rotation model

Data	Deg.	<i>Davies et al.</i> (1992)	Estimated
MGN			
4	20	0.282 ± 0.123	0.2793 0.123
4	30	0.2764 0.132	0.2681 0.132
4	40	0.249 ± 0.134	0.245 ± 0.134
4	50	0.237 ± 0.134	0.2554 0.136
4	60	0.2283 0.135	0.267 ± 0.136
4	90	0.225 ± 0.135	0.309 ± 0.138
5&6	20	0.299 ± 0.053	0.3063 0.054
5&6	30	0.2923 0.058	0.3034 0.059
5&6	40	0.2893 0.061	0.301 ± 0.062
5&6	50	0.296 ± 0.064	0.311 ± 0.065
5&6	60	0.308 ± 0.066	0.3234 0.067
5&6	90	0.319 ± 0.069	0.337 ± 0.070
All	20	0.2823 0.030	0.2843 0.030
All	30	0.287 ± 0.031	0.291 ± 0.031
All	40	0.2893 0.033	0.2954 0.033
All	50	0.292 ± 0.033	0.2993 0.033
All	60	0.292 ± 0.034	0.3004 0.035
All	90	0.301 ± 0.035	0.3204 0.036
		Spatial constraint	
All	90	0.3064 0.035	

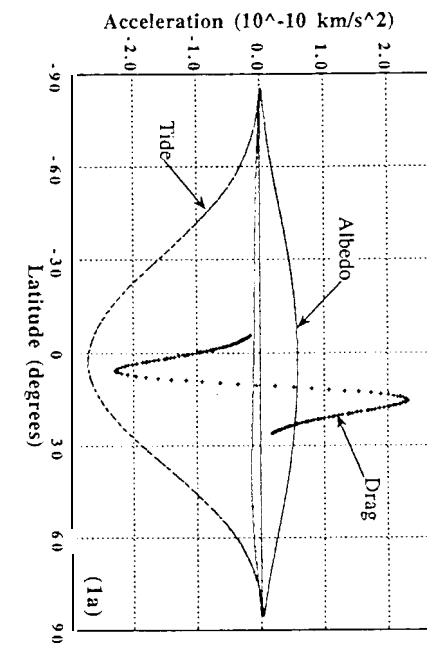
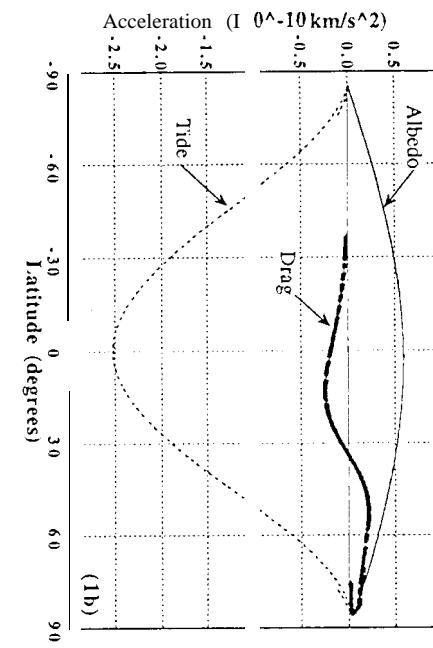
Errors are 1 standard deviation (1σ).

Table 2: Orbiting Spacecraft Sensitivity to k_2

Body	H $\times 10^{-8}$	v_s km/sec	k_2	$k_2 v_s H$ mm/sec
Mercury	45.06	3.14	0.35	0.50
Venus	7.15	7.33	0.25	0.13
Earth	5.09	7.91	0.30	0.12
Moon	123	1.68	0.030	0.06
Mars	1.02	3.55	0.14	0.005
10	2.1×10^4	1.81	1	380
Europa	1522	1.43	0.03	0.65
Titan	346	1.87	0.03	0.2

The planetary $H = (M_\odot/M)(R/a_\odot)^3$ (see eq. 4) except for Earth, for which the Moon is dominant and $H = (M_m/M)(R/a_m)^3$. For synchronously rotating satellites, this parameter depends on orbit eccentricity and for the radial tide is: $H = 3e(M_p/M)(R/a)^3$. Here $v_s = \sqrt{gR}$ is the surface orbiting velocity. Except for Earth and Moon, the Love numbers are estimates.

A spacecraft flyby of a body causes an across-track velocity change $\sim 1.5\pi k_2 H (v_0^2/v_{sp})(R/r_{sp}(\text{min}))^2 \hat{\mathbf{r}}_{sp}(\text{min}) \mathbf{r}_p$.



ionosphere and a representative neutral atmosphere. The four extremes of the diurnal and solar cycles have been represented based upon the typical mid-latitude ionosphere electron densities [Rich and Basu, 1985; Kelley, 1989]. Table 2 shows the residual bending angle error at 60 km altitude left after calibration for each of the four cases.

Pressure and Temperature

The nighttime solar minimum error is very small and the nighttime solar maximum and daytime solar minimum errors are sufficiently similar that only daytime solar maximum and nighttime solar maximum errors will be considered further. The impact of the daytime, solar maximum ionosphere on derived refractivity, pressure and temperature is shown in figures 15-17. Analogous results for nighttime solar maximum ionosphere conditions are shown in figures 18-20. The Abel and hydrostatic integrals in figures 15-20 were initiated with occultation data at 60 km. Refractivity errors increase approximately as the square root of Δz and fractional refractivity error therefore grows approximately exponentially with height. The geopotential height error in figure 16 indicates that residual ionosphere during daytime solar maximum conditions will limit accuracy above 25 km altitude. The peak temperature error of 6.5 K for daytime, solar maximum conditions occurs one Fresnel diameter below 60 km and a secondary peak of - 1.5K occurs near 43 km (Figure 17). The temperature error for all cases goes through zero near 50 km, consistent with the square root dependence of refractivity error on altitude (Section 3.2). The other three ionosphere cases do not appear to limit accuracy.

Discussion

The fractional errors in density, pressure and temperature all decrease rapidly with decreasing height because the density, pressure and temperature errors vary slowly relative to the exponential dependence of pressure and density on height. The negative bias apparent in the refractivity errors in Table 2 indicates that the calibration scheme defined by eq. (3.7.2), overcorrects slightly for the effects of the ionosphere and may be the one source of error which leaves a systematic bias signature in the retrievals. The temperature error behavior will be somewhat more complicated as indicated in figures 17 and 20.

The residual ionosphere errors in figures 15-20 can be improved using a better calibration scheme which leaves a residual zero-mean error. Higher order corrections to upward-looking ground-based GPS receiver observations have been developed to reduce errors by an order of magnitude [Bassiri and Hajj, 1993]. A similar higher order correction scheme should reduce ionospheric residual errors by at least a factor of 3. Nighttime observations at stratospheric attitudes should be very accurate for climate studies using the first order correction.

Caveats

The double Chapman layer representation of the F and E regions of the ionosphere used in the simulations presented here is realistic in a first order climatological sense. However, it contains neither horizontal nor small scale variations in structure. In the presence of horizontal variations, another source of error not considered here enters in the inversion process because the total bending is derived based on the assumption of spherical symmetry of the total index of refraction. This assumption is far less accurate in the ionosphere than in the neutral atmosphere due to the fact that the ray probes the ionosphere with a much longer scale than the neutral atmosphere. However, the error introduced by the non-spherical symmetry of the ionosphere is of order ($1/f^2$) or higher (simply because the total ionospheric bending is of order ($1/\lambda$) or higher); therefore, the linear combination